



Deposited via The University of Leeds.

White Rose Research Online URL for this paper:

<https://eprints.whiterose.ac.uk/id/eprint/129010/>

Version: Accepted Version

---

**Article:**

Zhang, K, Zhu, X, Wood, RA et al. (2018) Oxygenation of the Mesoproterozoic ocean and the evolution of complex eukaryotes. *Nature Geoscience*, 11 (5). pp. 345-350. ISSN: 1752-0894

<https://doi.org/10.1038/s41561-018-0111-y>

---

© 2018 Macmillan Publishers Limited, part of Springer Nature. This is a post-peer-review, pre-copyedit version of an article published in *Nature Geoscience*. The final authenticated version is available online at: <https://doi.org/10.1038/s41561-018-0111-y>. Uploaded in accordance with the publisher's self-archiving policy.

**Reuse**

Items deposited in White Rose Research Online are protected by copyright, with all rights reserved unless indicated otherwise. They may be downloaded and/or printed for private study, or other acts as permitted by national copyright laws. The publisher or other rights holders may allow further reproduction and re-use of the full text version. This is indicated by the licence information on the White Rose Research Online record for the item.

**Takedown**

If you consider content in White Rose Research Online to be in breach of UK law, please notify us by emailing [eprints@whiterose.ac.uk](mailto:eprints@whiterose.ac.uk) including the URL of the record and the reason for the withdrawal request.

1  
2  
3  
4  
5  
6  
7  
8  
9  
10  
11  
12  
13  
14  
15  
16  
17  
18  
19  
20

# **Oxygenation of the Mesoproterozoic ocean and the evolution of complex eukaryotes**

Kan Zhang<sup>1,2</sup>, Xiangkun Zhu<sup>1\*</sup>, Rachel A. Wood<sup>3</sup>, Yao Shi<sup>1</sup>, Zhaofu Gao<sup>1</sup>, Simon W. Poulton<sup>2</sup>

<sup>1</sup>MLR Key Laboratory of Isotope Geology, MLR Key Laboratory of Deep-Earth Dynamics, Institute of Geology, Chinese Academy of Geological Sciences, Beijing, 100037, China.

<sup>2</sup>School of Earth and Environment, University of Leeds, Leeds, LS2 9JT, UK.

<sup>3</sup>School of Geosciences, University of Edinburgh, Edinburgh, EH9 3FE, UK.

\*e-mail: xiangkunzhu@163.com

21 **Abstract**

22 **The Mesoproterozoic Era (1,600-1,000 million years ago; Ma) has long been considered a**  
23 **period of relative environmental stasis, with persistently low levels of atmospheric oxygen.**  
24 **There remains much uncertainty, however, over the evolution of ocean chemistry during this**  
25 **time period, which may have been of profound significance for the early evolution of**  
26 **eukaryotic life. Here, we present rare earth element, iron speciation and inorganic carbon**  
27 **isotope data to investigate the redox evolution of the 1,600-1,550 Ma Yanliao Basin, North**  
28 **China Craton. These data confirm that the ocean at the start of the Mesoproterozoic was**  
29 **dominantly anoxic and ferruginous. Significantly, however, we find evidence for a**  
30 **progressive oxygenation event starting at ~1,570 Ma, immediately prior to the occurrence of**  
31 **complex multicellular eukaryotes in shelf areas of the Yanliao Basin. Our study thus**  
32 **demonstrates that oxygenation of the Mesoproterozoic environment was far more dynamic**  
33 **and intense than previously envisaged, and establishes an important link between rising**  
34 **oxygen and the emerging record of diverse, multicellular eukaryotic life in the early**  
35 **Mesoproterozoic.**

36

37 The earliest definitive evidence for the evolution of eukaryotes occurs in late Paleoproterozoic  
38 marine sediments<sup>1,2</sup>, but the subsequent Mesoproterozoic has traditionally been perceived as a  
39 period of relative evolutionary stasis<sup>2</sup>. However, emerging evidence from several early  
40 Mesoproterozoic localities<sup>3,4,5</sup> increasingly supports a relatively high abundance and diversity of  
41 eukaryotic organisms by this time. Moreover, decimeter-scale, multicellular fossils have recently  
42 been discovered in early Mesoproterozoic (~1,560 Ma) shelf sediments from the Gaoyuzhuang  
43 Formation of the Yanliao Basin, North China Craton<sup>6</sup>. Although their precise affinity is unclear,  
44 the Gaoyuzhuang fossils most likely represent photosynthetic algae, and provide the strongest

45 evidence yet for the evolution of complex multicellular eukaryotes as early as the  
46 Mesoproterozoic<sup>6</sup>.

47 While molecular oxygen is required for eukaryotic synthesis<sup>7</sup>, the precise oxygen requirements  
48 of early multicellular eukaryotes, including the Gaoyuzhuang fossils, are unclear. This is  
49 exacerbated by the fact that recent reconstructions of oxygen levels across the Mesoproterozoic  
50 are highly variable, which has reignited the debate over the role of oxygen in early eukaryote  
51 evolution<sup>8,9,10,11</sup>. Thus, in addition to providing insight into the affinity of the Gaoyuzhuang fossils,  
52 a detailed understanding of the environmental conditions that prevailed in the Yanliao Basin  
53 would also inform on the nature of Earth surface oxygenation through the Mesoproterozoic.

54 Over recent years, understanding of Mesoproterozoic ocean chemistry has converged on a  
55 scenario whereby the deep ocean remained predominantly anoxic and iron-rich (ferruginous)  
56 beneath oxic surface waters, with widespread euxinic (anoxic and sulphidic) conditions being  
57 prevalent along biologically productive continental margins<sup>12,13,14</sup>. Other studies potentially  
58 indicate more variability in ocean redox during the Mesoproterozoic, with the suggestion that  
59 mid-depth waters may have become more oxygenated by ~1,400 Ma<sup>10,15,16</sup>. However, this  
60 possibility of enhanced ocean oxygenation significantly post-dates the occurrence of the  
61 Gaoyuzhuang fossils, and whether later Mesoproterozoic ocean oxygenation was widespread  
62 remains unclear. Indeed, in surface waters where photosynthetic eukaryotes had potential to thrive,  
63 evidence from organic carbon isotopes on the North China Craton suggests a very shallow  
64 chemocline from ~1,650-1,300 Ma<sup>17</sup>, while rare earth element (REE) data have been interpreted to  
65 reflect very low shallow water O<sub>2</sub> concentrations (~0.2 μM and below) throughout the  
66 Mesoproterozoic<sup>18</sup>.

67 Here, we present REE, Fe speciation and inorganic carbon isotope data for marine carbonates  
68 from the 1,600-1,550 Ma Yanliao Basin, to investigate ocean redox conditions in the basin where  
69 the Gaoyuzhuang fossils were discovered. Our data provide a more direct assessment of potential

70 links between the extent of environmental oxygenation and early eukaryote evolution, and suggest  
71 that the long-standing paradigm of the Mesoproterozoic as a period of prolonged environmental  
72 stasis requires conceptual reconsideration.

### 73 **Geological setting and samples**

74 The Jixian Section in the Yanliao Basin, 100 km east of Beijing, China, preserves ~9 km  
75 thickness of Proterozoic sedimentary rocks deposited atop Archean-Paleoproterozoic crystalline  
76 basement (see Supplementary Information). Our samples were collected from the ~1,600-1,550  
77 Ma Gaoyuzhuang Formation of the Jixian Section. The Gaoyuzhuang Formation is divided into  
78 four lithological members (Fig. 1), each of which comprises a shallowing-upward cycle consisting  
79 mainly of dolostone and limestone deposited in marine environments ranging from the deeper  
80 shelf slope to the supratidal/intertidal zone<sup>19,20</sup> (see Fig. 1 and Supplementary Information for full  
81 details of the depositional setting). U-Pb dating of zircons from tuff beds in the lower and upper  
82 horizons of the Zhangjiayu Member of the Gaoyuzhuang Formation (Fig. 1) gives ages of  $1,577 \pm$   
83  $12 \text{ Ma}^{21}$  and  $1,560 \pm 5 \text{ Ma}^{22}$ , respectively.

### 84 **Evaluating ocean redox chemistry**

85 With the exception of Cerium (Ce), REE are strictly trivalent in seawater and exhibit no  
86 intrinsic redox chemistry in most natural waters (the reduction of europium (Eu) from Eu(III) to  
87 Eu(II) during magmatic, metamorphic or hydrothermal process is an exception<sup>23</sup>, but is unlikely to  
88 have occurred in our samples). Solution complexation with ligands and surface adsorption to  
89 particles are fundamental processes controlling REE cycling in aquatic environments<sup>24</sup>.  
90 REE-carbonate ion complexes are the dominant dissolved species in seawater, with a systematic  
91 increase in complexation behaviour occurring from the light to heavy REE<sup>25</sup>. Particulate organic  
92 matter, and iron and manganese (oxyhydr)oxides, are the dominant carriers of REE, and the light  
93 REE (LREE) are preferentially scavenged by these particles compared to heavy REE (HREE)<sup>24</sup>.

94 These processes result in fractionation among REE, resulting in LREE depletion in oxic  
95 seawater<sup>24</sup>.

96 Yttrium (Y) and Holmium (Ho) act as a twin pair due to their similar charge and radius.  
97 Silicate rocks or clastic sedimentary rocks generally have chondritic Y/Ho values of ~28, implying  
98 no apparent fractionation of Y from Ho<sup>26</sup>. By contrast, seawater is generally characterized by  
99 super-chondritic Y/Ho ratio (>44), which results from Ho being scavenged faster than Y<sup>27</sup>. The  
100 differential behaviour of Cerium (Ce) is particularly useful as a water column redox indicator. Ce  
101 exists in either trivalent or tetravalent form, and in oxygenated water, soluble Ce<sup>3+</sup> tends to adsorb  
102 to Fe and/or Mn (oxyhydr)oxide minerals where oxidation to highly insoluble Ce<sup>4+</sup> is catalysed,  
103 resulting in a negative Ce anomaly in the water column<sup>28</sup>. Therefore, compared to ambient oxic  
104 seawater, marine particulates generally have higher LREE/HREE ratios, lower Y/Ho ratios, and  
105 smaller negative or even positive Ce anomalies<sup>24</sup>. When these particles settle into suboxic/anoxic  
106 deeper waters in a stratified ocean, REE become involved in redox-cycling, whereby particulate  
107 Mn, Fe and Ce undergo reductive dissolution, releasing scavenged trivalent REE back into  
108 solution<sup>29</sup>. This generates higher LREE/HREE ratios, lower Y/Ho ratios, and smaller negative or  
109 even positive Ce anomalies in the anoxic water column<sup>30,31</sup>. However, the original seawater REE  
110 patterns can be retained in coeval non-skeletal carbonates, thus providing fundamental information  
111 on ocean redox conditions<sup>31</sup>.

112 Diagenetic alteration and non-carbonate contamination (e.g., REE in clay minerals) are two  
113 factors that require consideration prior to the interpretation of REE data<sup>32</sup>. However,  
114 carbonate-REE are generally robust to post-depositional process such as diagenesis or  
115 dolomitization<sup>33</sup>, and most samples evaluated in our study have experienced little diagenetic  
116 recrystallization and only very early dolomitization (based on petrographic features observed  
117 under optical microscopy and cathodoluminescence; see Supplementary Information). Although  
118 some dolomites from the fourth member of the Gaoyuzhuang Formation show a unimodal,

119 nonplanar texture which may reflect late burial dolomitization, these samples retain typical  
120 seawater-like REE patterns (Fig. 1a), suggesting little modification of REE patterns. To address  
121 the potential for non-carbonate contamination, we utilized a sequential dissolution method for  
122 REE using dilute acetic acid (see Methods), which enables REE in carbonates to be specifically  
123 targeted<sup>34</sup>. In addition, no obvious co-variation was observed between Al, Sc, or Th (as indicators  
124 of detrital materials) and various REE parameters (e.g., the sum of REE ( $\Sigma$ REE), Y/Ho ratios, the  
125 fractionation between LREE and HREE ( $Pr_n/Er_n$ ), or Ce anomalies ( $Ce_n/Ce_n^*$ ); see Supplementary  
126 Fig. 5). These observations provide strong support for preservation and extraction of primary  
127 seawater REE signals<sup>32</sup>.

128 The PAAS-normalized REE patterns of the Gaoyuzhuang Formation carbonates show  
129 systematic variability which can be categorized into six groups (Fig. 1a). Carbonates from ~0-650  
130 m, including the Guandi Member, the Sangshu'an Member, and the lower part of the Zhangjiayu  
131 Member of the Gaoyuzhuang Formation (Group GYZ-1, GYZ-2, GYZ-3-1), show marine REE  
132 patterns that are generally not typical of oxic seawater: middle REE (MREE) enrichment, LREE  
133 enrichment or nearly flat REE patterns, near chondritic or slightly higher Y/Ho ratios, and absent  
134 (or small) Ce anomalies. Samples from ~650-800 m (Group GYZ-3-2) show variable REE  
135 patterns, some of which start to show REE patterns and negative Ce anomalies typical of oxic  
136 seawater. Samples from 800 m to the top of the section (Group GYZ-3-3 and GYZ-4) show  
137 typical oxic marine REE patterns with negative Ce anomalies ( $Ce_n/Ce_n^* = 0.69-0.92$ ). These  
138 temporal trends in REE patterns record the long-term redox evolution of the Yanliao Basin.

139 In addition to the REE data, we also utilized Fe speciation as an independent redox indicator.  
140 Fe speciation is a well-calibrated technique for identifying anoxia in the water column, and is the  
141 only technique that enables ferruginous conditions to be directly distinguished from euxinia<sup>14,35</sup>.  
142 Besides application to ancient fine-grained siliciclastic marine sediments, Fe speciation can also  
143 be successfully applied to carbonate-rich sediments<sup>31,36,37</sup>, providing samples contain sufficient

144 total Fe ( $Fe_T > 0.5$  wt%) to produce robust interpretations that are not skewed by the potential for  
145 Fe mobilization during late-stage diagenesis or deep burial dolomitization<sup>38</sup>. Hence, we only  
146 applied Fe speciation to samples with  $Fe_T > 0.5$  wt% (Fig. 1), and in addition, our samples were  
147 screened for potential modification of primary signals by deep burial dolomitisation (see  
148 Supplementary Information).

149 Fe speciation defines an Fe pool that is considered highly reactive ( $Fe_{HR}$ ) towards biological  
150 and abiological reduction under anoxic conditions, including carbonate-associated Fe ( $Fe_{carb}$ ),  
151 ferric oxides ( $Fe_{ox}$ ), magnetite ( $Fe_{mag}$ ) and pyrite ( $Fe_{py}$ )<sup>39</sup>. Sediments deposited from anoxic waters  
152 commonly have  $Fe_{HR}/Fe_T > 0.38$ , whereas ratios below 0.22 are generally considered to provide a  
153 robust indication of oxic depositional conditions<sup>14</sup>. For samples showing evidence of anoxic  
154 deposition (i.e.,  $Fe_{HR}/Fe_T > 0.38$ ), ferruginous conditions can be distinguished from euxinia by the  
155 extent of pyritization of the  $Fe_{HR}$  pool, with  $Fe_{py}/Fe_{HR} > 0.7-0.8$  indicating euxinia, and  $Fe_{py}/Fe_{HR}$   
156  $< 0.7$  indicating ferruginous conditions<sup>35,40,41</sup>.

157 From 0-800 m in the Gaoyuzhuang Formation, 33 out of 54 samples had  $Fe_T > 0.5$  wt% and  
158 were deemed suitable for Fe speciation<sup>38</sup>, whereas all samples higher in the succession contained  
159  $< 0.5$  wt% (Fig. 1c). The samples from 0-800 m show clear evidence for water column anoxia,  
160 with high  $Fe_{HR}/Fe_T > 0.38$ . Furthermore, low  $Fe_{py}/Fe_{HR}$  ratios support ferruginous, rather than  
161 euxinic, depositional conditions (Fig. 1d). Iron speciation also reveals a significant enrichment in  
162 ferric (oxyhydr)oxide minerals in GYZ-3-2 sediments, rather than reduced or mixed valence  $Fe_{HR}$   
163 phases, with  $Fe_{ox}$  increasing up to 65% of the total  $Fe_{HR}$  pool (Fig. 1e) coincident with the first  
164 development of REE patterns typical of oxic seawater.

165 Carbonates were also analyzed for their inorganic carbon isotope ( $\delta^{13}C_{carb}$ ) compositions.  
166 Values vary from -2.85‰ to +0.54‰ and are entirely consistent with previous analyses from other  
167 parts of the Yanliao Basin (Fig. 2). We interpret these  $\delta^{13}C_{carb}$  data to reflect contemporaneous  
168 seawater signatures with minimal diagenetic overprint (see Supplementary Information).

169 Throughout much of the section there is a relatively narrow range in  $\delta^{13}\text{C}_{\text{carb}}$ , but a rapid,  
170 basin-wide, negative carbon isotope excursion (to values as low as  $-2.85\text{‰}$ ) occurs in the lower  
171 part of the Zhangjiayu Member of the Gaoyuzhuang Formation.

## 172 **Oxygenation of the early Mesoproterozoic ocean**

173 Our REE and Fe speciation data provide strong, independent evidence for anoxic depositional  
174 conditions across the lower two members, and the basal part of the Zhangjiayu Member, of the  
175 Gaoyuzhuang Formation (GYZ-1, GYZ-2 and GYZ-3-1 in Fig. 1). These samples span a  
176 significant range in water depth, from shallow to deeper, distal environments<sup>19,20</sup>, suggesting that  
177 ferruginous conditions were a prevalent feature of the water column throughout the basin,  
178 including in very shallow waters (Fig. 3a). Above this, samples from  $\sim 650\text{--}800\text{ m}$  (GYZ-3-2 in Fig.  
179 1) have variable REE features, suggesting precipitation around a transitional redox zone. In  
180 support of this, Fe speciation data continue to record ferruginous conditions, implying a redox  
181 boundary between ferruginous deeper waters and shallower oxic waters. Moreover, an increase in  
182 the magnitude of negative Ce anomalies is apparent across this transitional zone (Fig. 1b), which  
183 also records a significant increase in the preservation of ferric (oxyhydr)oxide minerals in the  
184 sediment (Fig. 1e).

185 In combination, these observations suggest that our data capture a major transition in water  
186 column oxygenation, which resulted in extensive precipitation of Fe (oxyhydr)oxide minerals at  
187 the chemocline as ferruginous deeper waters became oxygenated (which is supported by the  
188 significant increase in total Fe across this interval; Fig. 1c). Indeed, this transitional redox zone  
189 occurs as water depth increases to almost the maximum observed in the succession (Fig. 1),  
190 suggesting that a significant rise in surface water oxygen levels resulted in a major deepening of  
191 the chemocline, as depicted in Fig. 3b.

192 REE systematics then support the persistence of well-oxygenated waters throughout the

193 overlying succession, from deep basinal waters, through fluctuating water depths, to very shallow  
194 waters. If dissolved oxygen content remained constant as water depth shallowed through time, a  
195 change from more negative (in deeper waters) to less negative (in shallower waters) Ce anomalies  
196 would naturally occur, due to preferential desorption of light REE relative to Ce(IV) at depth in  
197 the water column<sup>42</sup>. Therefore, the relatively stable negative Ce anomalies (and the one sample  
198 with a large negative anomaly) as water depth shallows from 800 m to the top of the Gaoyuzhuang  
199 Formation (Fig. 1b) imply continued progressive oxygenation of the water column (Fig. 3c). The  
200 very low Fe<sub>T</sub> content of these samples following large scale drawdown of water column Fe in unit  
201 GYZ-3-2 (Fig. 1) is also entirely consistent with an absence of Fe<sub>HR</sub> (and Fe<sub>py</sub>) enrichments due to  
202 persistent water column oxygenation<sup>38</sup>.

203 Our reconstruction of anoxic ferruginous water column conditions in very shallow waters of  
204 the lower Gaoyuzhuang Formation (Fig. 3a) is consistent with previous studies suggesting very  
205 low surface water oxygenation in the Mesoproterozoic<sup>17</sup>. However, we also find clear evidence for  
206 a progressive oxygenation ‘event’ beginning at ~1,570 Ma. REE and Fe speciation data are,  
207 however, considered to record local to regional water column redox conditions. To place our  
208 observations in the more widespread context of the entire Yanliao Basin, we also consider carbon  
209 isotope systematics from the Jixian Section and elsewhere in the basin. A prominent negative  
210  $\delta^{13}\text{C}_{\text{carb}}$  excursion, lasting ~1.6 myr (assuming a constant depositional rate), is apparent throughout  
211 the Yanliao Basin at ~1,570 Ma (Fig. 2), coincident with the onset of the oxygenation ‘event’, as  
212 recorded independently by our geochemical data. This excursion has previously been attributed to  
213 diagenetic alteration<sup>43</sup>, but more detailed isotopic studies have suggested that the excursion  
214 reflects the development of anoxic bottom waters in deeper basinal environments, which may have  
215 resulted in enhanced heterotrophic remineralization under anoxic conditions<sup>19</sup>. However, these  
216 previous studies lacked the environmental context afforded by our redox evaluation of the water  
217 column, which suggests that, by contrast, the excursion is linked to the development of oxic,

218 rather than anoxic, conditions.

219 Based on our data, we consider two potential mechanisms to explain the negative  $\delta^{13}\text{C}_{\text{carb}}$   
220 excursion. The first mechanism would require a widespread decline in organic carbon burial, but  
221 this is inconsistent with total organic carbon (TOC) data, which shows an increase from  $<0.1$  wt%  
222 below the excursion to  $\sim 0.5$  wt% during the excursion (Supplementary Fig. 7). Instead, we suggest  
223 that the negative  $\delta^{13}\text{C}_{\text{carb}}$  excursion is directly related to widespread oxygenation in the basin, and  
224 likely reflects the oxidation of a  $\delta^{13}\text{C}$  depleted pool of dissolved organic carbon and/or methane at  
225 the redoxcline. The  $\delta^{13}\text{C}_{\text{carb}}$  record of early Mesoproterozoic successions in the Yanliao Basin also  
226 shows a gentle long-term increase to more positive values above the negative isotope excursion  
227 (Fig. 2; ref 44), which is also consistent with the progressive longer-term increase in oxygenation  
228 indicated by our REE data. This would be consistent with the emerging evidence for possible  
229 deeper water oxygenation recorded in marine sediments from the  $\sim 1,400$  Ma Kaltasy Formation,  
230 Russia<sup>16</sup>, and in the  $\sim 1,400$ - $1,320$  Ma Xiamaling Formation, North China<sup>10,15</sup>. These observations  
231 suggest that our data may capture the onset of a major, global rise in Mesoproterozoic Earth  
232 surface oxygenation, which contrasts with the persistent low-oxygen condition often advocated for  
233 this time period<sup>8,9,17,18</sup>.

## 234 **Implications for eukaryote evolution**

235 The complex eukaryotes of the Gaoyuzhuang Formation (Fig. 1) are found in the Zhangjiayu  
236 Member<sup>6</sup>, shortly after the onset of the oxygenation ‘event’ recorded by our geochemical data. In  
237 addition, the Gaoyuzhuang fossils are found near storm wave base on the shelf (Fig. 3b)<sup>6</sup>,  
238 suggesting that rising oxygen levels and a concomitant deepening of the oxycline created the  
239 environmental stability required for their evolution. This reinforces the role of oxygen as an  
240 evolutionary driver in the Mesoproterozoic, and provides support for the suggestion that these  
241 complex eukaryotes were likely involved in aerobic respiration and photosynthesis<sup>6</sup>. While

242 Gaoyuzhuang-type fossils have not yet been discovered elsewhere, several other early  
243 Mesoproterozoic successions, including the Ruyang Group (~1,750-1,400 Ma) in the southwestern  
244 margin of the North China Craton<sup>3</sup>, the Kotuikan Formation (~1,500 Ma) on the northern Siberia  
245 Platform<sup>5</sup>, and the Roper Group (~1,500 Ma) in northern Australia<sup>4</sup>, have been reported to  
246 preserve a relatively high abundance and diversity of eukaryotic organisms, in contrast to older  
247 strata. This suggests that chemical and biological evolution during the Mesoproterozoic were  
248 likely intrinsically linked, and far from static, on a global scale.

249 In summary, the early Mesoproterozoic Yanliao Basin records an important step-change in  
250 Earth's oxygenation history, which was most likely linked to atmospheric oxygenation. The  
251 emerging evidence from the North China Craton and elsewhere<sup>10,15,16</sup> suggests that the progressive  
252 oxygenation 'event' recorded by our data may have been of global significance, with major  
253 implications for eukaryote evolution. While further detailed study of other successions is required  
254 to evaluate spatial and temporal constraints on early Mesoproterozoic oxygenation, our data build  
255 upon emerging evidence from the fossil record, to suggest that environmental change was likely  
256 considerably more dynamic than previously recognised during the far from 'boring'  
257 Mesoproterozoic Era.

258

## 259 **References**

- 260 1. Rasmussen, B., Fletcher, I. R., Brocks, J. J. & Kilburn, M. R. Reassessing the first appearance  
261 of eukaryotes and cyanobacteria. *Nature* **455**, 1101-1104 (2008).
- 262 2. Knoll, A. H., Javaux, E. J., Hewitt, D. & Cohen, P. Eukaryotic organisms in Proterozoic  
263 oceans. *Philos Trans R Soc Lond B Biol Sci* **361**, 1023-1038 (2006).
- 264 3. Agić, H., Moczydłowska, M. & Yin, L. Diversity of organic-walled microfossils from the  
265 early Mesoproterozoic Ruyang Group, North China Craton - a window into the early

- 266 eukaryote evolution. *Precambrian Research* **297**, 101-130 (2017).
- 267 4. Javaux, E. J., Knoll, A. H. & Walter, M. R. Morphological and ecological complexity in early  
268 eukaryotic ecosystems. *Nature* **412**, 66-69 (2001).
- 269 5. Vorob'eva, N. G., Sergeev, V. N. & Petrov, P. Y. Kotuikan Formation assemblage: A diverse  
270 organic-walled microbiota in the Mesoproterozoic Anabar succession, northern Siberia.  
271 *Precambrian Research* **256**, 201-222 (2015).
- 272 6. Zhu, S. et al. Decimetre-scale multicellular eukaryotes from the 1.56-billion-year-old  
273 Gaoyuzhuang Formation in North China. *Nat Commun* **7**, 11500 (2016).
- 274 7. Summons, R. E., Bradley, A. S., Jahnke, L. L. & Waldbauer, J. R. Steroids, triterpenoids and  
275 molecular oxygen. *Philos Trans R Soc Lond B Biol Sci* **361**, 951-968 (2006).
- 276 8. Lyons, T. W., Reinhard, C. T. & Planavsky, N. J. The rise of oxygen in Earth's early ocean and  
277 atmosphere. *Nature* **506**, 307-315 (2014).
- 278 9. Planavsky, N. J. et al. Low Mid-Proterozoic atmospheric oxygen levels and the delayed rise of  
279 Animals. *Science* **346**, 635-638 (2014).
- 280 10. Zhang, S. et al. Sufficient oxygen for animal respiration 1,400 million years ago. *Proc Natl*  
281 *Acad Sci* **113**, 1731-1736 (2016).
- 282 11. Daines, S. J., Mills, B. J. & Lenton, T. M. Atmospheric oxygen regulation at low Proterozoic  
283 levels by incomplete oxidative weathering of sedimentary organic carbon. *Nat Commun* **8**,  
284 14379 (2017).
- 285 12. Poulton, S. W., Fralick, P. W. & Canfield, D. E. Spatial variability in oceanic redox structure  
286 1.8 billion years ago. *Nature Geoscience* **3**, 486-490 (2010).
- 287 13. Planavsky, N. J. et al. Widespread iron-rich conditions in the mid-Proterozoic ocean. *Nature*  
288 **477**, 448-451 (2011).
- 289 14. Poulton, S. W. & Canfield, D. E. Ferruginous Conditions: A Dominant Feature of the Ocean  
290 through Earth's History. *Elements* **7**, 107-112 (2011).

- 291 15. Wang, X. et al. Oxygen, climate and the chemical evolution of a 1400 million year old  
292 tropical marine setting. *American Journal of Science* **317**, 861-900 (2017).
- 293 16. Sperling, E. A. et al. Redox heterogeneity of subsurface waters in the Mesoproterozoic ocean.  
294 *Geobiology* **12**, 373-386 (2014).
- 295 17. Luo, G. et al. Shallow stratification prevailed for ~1700 to ~1300 Ma ocean: Evidence from  
296 organic carbon isotopes in the North China Craton. *Earth and Planetary Science Letters* **400**,  
297 219-232 (2014).
- 298 18. Tang, D., Shi, X., Wang, X. & Jiang, G. Extremely low oxygen concentration in  
299 mid-Proterozoic shallow seawaters. *Precambrian Research* **276**, 145-157 (2016).
- 300 19. Guo, H. et al. Sulfur isotope composition of carbonate-associated sulfate from the  
301 Mesoproterozoic Jixian Group, North China: Implications for the marine sulfur cycle.  
302 *Precambrian Research* **266**, 319-336 (2015).
- 303 20. Mei, M. Preliminary study on sequence-stratigraphic position and origin for Molar-tooth  
304 structure of the Gaoyuzhuang Formation of Mesoproterozoic at Jixian section in Tianjin.  
305 *Journal of Palaeogeography* **7**, 437-447 (2005).
- 306 21. Tian, H. et al. Zircon LA-MC-ICPMS U-Pb dating of tuff from Mesoproterozoic  
307 Gaoyuzhuang Formation in Jixian Country of North China and its geological significance.  
308 *Acta Geoscientica Sinica* **36**, 647-658 (2015).
- 309 22. Li, H. et al. Further constraints on the new subdivision of the Mesoproterozoic stratigraphy in  
310 the northern North China Craton. *Acta Petrologica Sinica* **26**, 2131-2140 (2010).
- 311 23. Michard, A., Albarède, F., Michard, G., Minster, J. F. & Charlou, J. L. Rare-earth elements  
312 and uranium in high-temperature solutions from East Pacific Rise hydrothermal vent field (13  
313 °N). *Nature* **303**, 795-797 (1983).
- 314 24. Sholkovitz, E. R., Landing, W. M. & Lewis, B. L. Ocean particle chemistry: The fractionation  
315 of rare earth elements between suspended particles and seawater. *Geochimica et*

- 316 *Cosmochimica Acta* **58**, 1567-1579 (1994).
- 317 25. Cantrell, K. J. & Byrne, R. H. Rare earth element complexation by carbonate and oxalate ions.  
318 *Geochimica et Cosmochimica Acta* **51**, 597-605 (1987).
- 319 26. Bau, M. Controls on the fractionation of isovalent trace elements in magmatic and aqueous  
320 systems: evidence from Y/Ho, Zr/Hf, and lanthanide tetrad effect. *Contrib Mineral Petrol* **123**,  
321 323-333 (1996).
- 322 27. Nozaki, Y., Zhang, J. & Amakawa, H. The fractionation between Y and Ho in marine  
323 environment. *Earth and Planetary Science Letters* **148**, 329-340 (1997).
- 324 28. Bau, M. & Koschinsky, A. Oxidative scavenging of cerium on hydrous Fe oxides: Evidence  
325 from the distribution of rare earth elements and yttrium between Fe oxides and Mn oxides in  
326 hydrogenetic ferromanganese crusts. *Geochemical Journal* **43**, 37-47 (2009).
- 327 29. German, C. R., Holliday, B. P. & Elderfield, H. Redox cycling of rare earth elements in the  
328 suboxic zone of the Black Sea. *Geochimica et Cosmochimica Acta* **55**, 3553-3558 (1991).
- 329 30. Bau, M., Moller, P. & Dulski, P. Yttrium and lanthanides in eastern Mediterranean seawater  
330 and their fractionation during redox-cycling. *Marine Chemistry* **56**, 123-131 (1997).
- 331 31. Tostevin, R. et al. Low-oxygen waters limited habitable space for early animals. *Nat Commun*  
332 **7**, 12818 (2016).
- 333 32. Nothdurft, L. D., Webb, G. E. & Kamber, B. S. Rare earth element geochemistry of Late  
334 Devonian reefal carbonates, Canning Basin, Western Australia: confirmation of a seawater  
335 REE proxy in ancient limestones. *Geochimica et Cosmochimica Acta* **68**, 263-283 (2004).
- 336 33. Banner, J. L., Hanson, G. N. & Meyers, W. J. Rare earth elements and Nd isotopic variations  
337 in regionally extensive dolomites from the Burlington-Keokuk Formation (Mississippian):  
338 Implications for REE mobility during carbonate diagenesis. *Journal of Sedimentary Petrology*  
339 **58**, 415-432 (1988).
- 340 34. Zhang, K., Zhu, X. & Yan, B. A refined dissolution method for rare earth element studies of

- 341 bulk carbonate rocks. *Chemical Geology* **412**, 82-91 (2015).
- 342 35. Poulton, S. W., Fralck, P. W. & Canfield, D. E. The transition to a sulphidic ocean ~1.84  
343 billion years ago. *Nature* **431**, 173-177 (2004).
- 344 36. Clarkson, M. O. et al. Dynamic anoxic ferruginous conditions during the end-Permian mass  
345 extinction and recovery. *Nat Commun* **7**, 12236 (2016).
- 346 37. Wood, R. A. et al. Dynamic redox conditions control late Ediacaran metazoan ecosystems in  
347 the Nama Group, Namibia. *Precambrian Research* **261**, 252-271 (2015).
- 348 38. Clarkson, M. O., Poulton, S. W., Guilbaud, R. & Wood, R. A. Assessing the utility of Fe/Al  
349 and Fe-speciation to record water column redox conditions in carbonate-rich sediments.  
350 *Chemical Geology* **382**, 111-122 (2014).
- 351 39. Poulton, S. W. & Canfield, D. E. Development of a sequential extraction procedure for iron:  
352 implications for iron partitioning in continentally derived particulates. *Chemical Geology* **214**,  
353 209-221 (2005).
- 354 40. Poulton, S. W. & Raiswell, R. The low-temperature geochemical cycle of iron: From  
355 continental fluxes to marine sediment deposition. *American Journal of Science* **302**, 774-805  
356 (2002).
- 357 41. Raiswell, R. & Canfield, D. E. Sources of iron for pyrite formation in marine sediments.  
358 *American Journal of Science* **298**, 219-245 (1998).
- 359 42. Ling, H. et al. Cerium anomaly variations in Ediacaran–earliest Cambrian carbonates from the  
360 Yangtze Gorges area, South China: Implications for oxygenation of coeval shallow seawater.  
361 *Precambrian Research* **225**, 110-127 (2013).
- 362 43. Li, R., Chen, J., Zang, S. & Chen, Z. Secular variations in carbon isotopic compositions of  
363 carbonates from Proterozoic successions in the Ming Tombs Section of the North China  
364 Platform. *Journal of Asian Earth Sciences* **22**, 329-341 (2003).
- 365 44. Guo, H. et al. Isotopic composition of organic and inorganic carbon from the Mesoproterozoic

366 Jixian Group, North China: Implications for biological and oceanic evolution. *Precambrian*  
367 *Research* **224**, 169-183 (2013).

368

### 369 **Acknowledgements**

370 This work was supported by NSFC Grant 41430104 and CAGS Research Fund YYWF201603 to  
371 X.K.Z., a China Scholarship Council award to K.Z. and a China Geological Survey Grant  
372 DD20160120-04 to Bin Yan. S.W.P. acknowledges support from a Royal Society Wolfson  
373 Research Merit Award. We thank Linzhi Gao and Pengju Liu for field guidance, and Fuqiang Shi,  
374 Chao Tang, Xi Peng, Chenxu Pan, Nina Zhao, Chuang Bao, Zilong Zhou and Yueling Guo for  
375 field work assistance. We acknowledge Feipeng Xu and Miao Lv for assistance in elemental  
376 analysis, Yijun Xiong for help with Fe speciation experiments, Yanan Shen, Kefan Chen and Wei  
377 Huang for carbon isotope analyses, and Fred Bowyer for assistance with cathodoluminescence.  
378 We also express our thanks to Jin Li, Da Li, Yuan He, Jianxiong Ma, Xinjie Zou and Kun Du for  
379 logistical support.

### 380 **Author contributions**

381 X.K.Z. designed the project. X.K.Z., K.Z., Y.S., Z.F.G. did fieldwork and collected samples. K.Z.  
382 carried out elemental and Fe speciation analyses. R.A.W. provided expertise in the evaluation of  
383 carbonate diagenesis. X.K.Z., K.Z. and S.W.P. interpreted the data, and K.Z., S.W.P. and X.K.Z.  
384 wrote the paper, with additional input from all co-authors.

### 385 **Competing financial interests**

386 The authors declare no competing financial interests.

### 387 **Figure captions**

388 **Figure 1: Summary of sedimentary facies (SF) and geochemical signals for carbonates from**

389 **the Gaoyuzhuang Formation, Jixian Section.** (a) PAAS-normalized REE patterns categorized  
390 into six groups. (b) Cerium anomaly profile (see Supplementary Information for calculation  
391 details). (c) Total Fe ( $Fe_T$ ) profile (analytical precision is within the size of the symbols). (d) Fe  
392 speciation results (see text for details). (e)  $Fe_{ox}/Fe_{HR}$  profile. Sea level reached its highest around  
393 the middle Gaoyuzhuang Formation<sup>19,20</sup>.

394

395 **Figure 2: Compilation of inorganic carbon isotope ( $\delta^{13}C_{carb}$ ) data for the Gaoyuzhuang**  
396 **Formation across the Yanliao Basin.** Jixian Section (this study); Pingquan Section (ref 44); Ming  
397 Tombs Section (ref 43) (see Supplementary Fig. 1a for sample locations). Analytical precision is  
398 within the size of the symbols.

399

400 **Figure 3: Cartoon depicting the redox evolution of the early Mesoproterozoic Yanliao Sea.**  
401 Three stages are depicted, including the relative position of carbonates analyzed for the present  
402 study: (a) In the earliest Mesoproterozoic, seawater was anoxic and ferruginous with a very  
403 shallow chemocline; (b) The chemocline deepened, likely to below storm wave base, around the  
404 middle of Gaoyuzhuang Formation, in response to the onset of oxygenation. The increase in  
405 shallow water oxygenation coincides with the presence of decimeter-scale, complex multicellular  
406 eukaryotes; (c) The extent of ocean oxygenation continued to increase with time.

407

## 408 **Methods**

### 409 **Rare Earth Elements**

410 The chemical dissolution of REE was carried out in a class 100 ultra-clean laboratory. The  
411 dissolution method applied has been reported elsewhere<sup>34</sup>. Briefly, the technique initially dissolves  
412 30-40% of total carbonate, followed by a subsequent extraction of the next 30-40% of total

413 carbonate using dilute acetic acid (0.5 mol/L), which was sampled for REE and considered to best  
414 represent that of the carbonate source water. Elemental analysis, including REE, Th, Sc, Ca, Mg  
415 and Al in carbonate leachates, was conducted via ICP-MS and ICP-OES, with replicate extractions  
416 giving a RSD of less than 3% for these elements.

#### 417 **Fe-speciation and total Fe**

418 Fe-speciation extraction was performed using standard sequential extraction protocols<sup>39</sup>. Iron in  
419 carbonate minerals ( $Fe_{carb}$ ) was extracted with a sodium acetate solution at pH 4.5, for 48 h at  
420 50°C; Iron (oxyhydr)oxide minerals ( $Fe_{ox}$ ) were then extracted with a sodium dithionite solution at  
421 pH 4.8 for 2 h at room temperature; Finally, magnetite Fe ( $Fe_{mag}$ ) was extracted with an  
422 ammonium oxalate solution for 6 h at room temperature. All Fe concentrations were measured via  
423 atomic absorption spectrometry (AAS) with replicate extractions giving a RSD of <5% for all  
424 phases. Total iron ( $Fe_T$ ) were determined by one of two methods: 1. X-Ray Fluorescence; 2. A  
425  $HNO_3$ -HF- $HClO_4$  digest on ashed samples (overnight at 550°C) followed by AAS analysis. Pyrite  
426 iron ( $Fe_{py}$ ) was calculated on the basis of the weight percentage of sulphur extracted during  
427 chromous chloride distillation<sup>45</sup>, with a RSD of <5%.

#### 428 **Inorganic carbon isotopes**

429 To determine  $\delta^{13}C_{carb}$ , carbonate powders of ~150  $\mu g$  were first reacted with anhydrous phosphoric  
430 acid at 70°C to extract  $CO_2$  using a KEIL IV carbonate device. The produced  $CO_2$  was then  
431 purified stepwise and ultimately introduced into a Finnigan MAT 253 mass spectrometer. Carbon  
432 isotope determinations were performed using a dual-inlet mode against an in-house standard  
433 reference gas in the mass spectrometer. All values are reported as  $\delta^{13}C_{carb}$  relative to the Vienna  
434 Peedee Belemnite (VPDB) standard. The precision is better than 0.06‰ based on replicate  
435 analyses of the Chinese national standard GBW04416 ( $\delta^{13}C = 1.61 \pm 0.03\text{‰}$ ).

436 **Data availability**

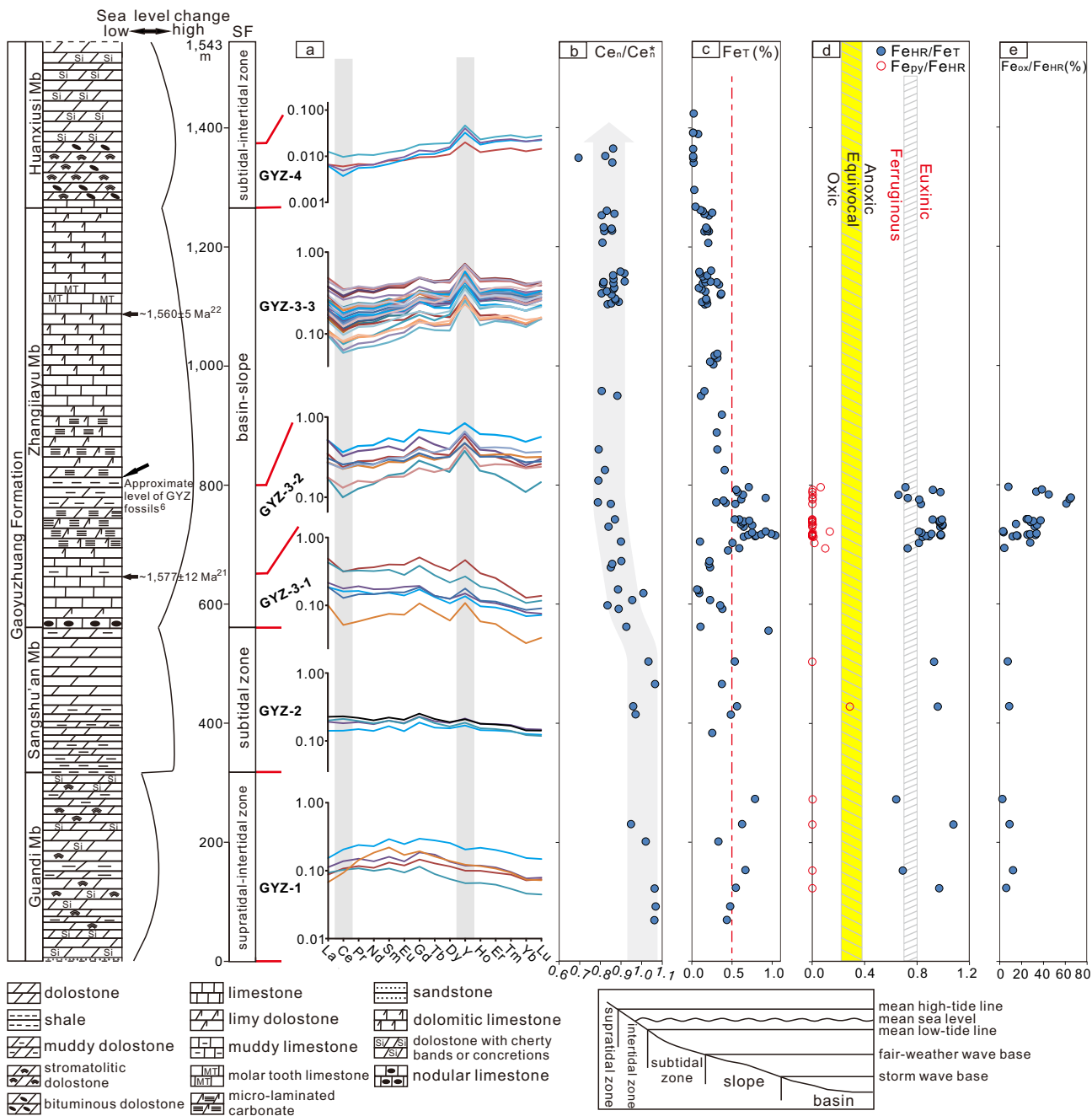
437 The authors declare that the data supporting the findings of this study are available within the  
438 article and its supplementary information files.

439 **References in Methods**

440 45. Canfield, D. E., Raiswell, R., Westrich, J. T., Reaves, C. M. & Berner, R. A. The use of  
441 chromium reduction in the analysis of reduced inorganic sulfur in sediments and shales.  
442 *Chemical Geology* **54**, 149-155 (1986).

443

444 Correspondence and requests for materials should be addressed to Xiangkun Zhu  
445 (xiangkunzhu@163.com).



Height(m) ● Jixian Section △ Pingquan Section ■ Ming Tombs Section

